Hindawi
Journal of Spectroscopy
Volume 2019, Article ID 5037836, 18 pages
https://doi.org/10.1155/2019/5037836

Research Article

Evolution Mechanism of Macromolecular Structure in Coal during Heat Treatment: Based on FTIR and XRD In Situ Analysis Techniques

Dun Wu [1,2,3] **and Wenyong Zhang** [3]

[1]*School of Earth and Space Sciences, University of Science and Technology of China, CAS Key Laboratory of Crust-Mantle Materials and Environment, Hefei, Anhui 230026, China*
[2]*Research Center of Coal Resources Safe Mining and Clean Utilization, LiaoNing Technical University, Fuxin 125105, Liaoning, China*
[3]*Exploration Research Institute, Anhui Provincial Bureau of Coal Geology, Hefei, Anhui 23008, China*

Correspondence should be addressed to Dun Wu; wudun@ustc.edu.cn

Received 14 October 2018; Revised 23 December 2018; Accepted 5 March 2019; Published 3 April 2019

Academic Editor: Christoph Krafft

Owing to the complexity and heterogeneity of coal during pyrolysis, the ex situ analytical techniques cannot accurately reflect the real coal pyrolysis process. In this study, according to the joint investigation of Fourier-transform infrared spectroscopy (FTIR) and X-ray diffraction (XRD), the structural evolution characteristics of lignite-subbituminous coal-bituminous coal-anthracite series under heat treatment were discussed in depth. The results of the infrared spectrum of coal show that the different functional groups of coal show different changes with the increase of coal rank before pyrolysis experiment. Based on in situ infrared spectroscopy experiments, it was found that the infrared spectrum curves of the same coal sample have obvious changes at different pyrolysis temperatures. As a whole, when the pyrolysis temperature is between 400 and 500°C, the coal structure can be greatly changed. By fitting the infrared spectrum curve, the infrared spectrum parameters of coal were obtained. With the change of temperature, these parameters show regular changes in coal with different ranks. In the XRD study of coal, the absorption intensity of the diffraction peak (002) of coal increases with increasing coal rank. The XRD patterns of coal have different characteristics at different pyrolysis temperatures. Overall, the area of (002) diffraction peak of the same coal sample increases obviously with the increase of temperature. The XRD structural parameter of coal was obtained by using the curve fitting method. The changing process of two parameters (interlayer spacing (d_{002}) and stacking height (L_c)) can be divided into two main stages, but the average lateral size (L_a) does not change significantly and remains at the 2.98 ± 0.09 nm. In summary, the above two technologies complement each other in the study of coal structure. The temperature range of both experiments is different, but the XRD parameters of coal with different ranks are reduced within the temperature range of less than 500°C, which reflects that the size of coal-heated aromatic ring lamellae is reduced and the distance between lamellae is also reduced, indicating that the degree of condensation of coal aromatic nuclei may be increased. Correspondingly, the FTIR parameters of coal also reflect that, with increasing temperature, the side chains of coal are constantly cracked, the oxygen-containing functional groups are reduced, and the degree of aromatization of coal may be increased.

1. Introduction

The integrally structural arrangement of coal increases with proceeding coalification up to the formation of organic macromolecules of flat shape with carbon atoms in the central part [1–3]. During coalification, the size of coal molecules increases as well as the degree of their ordering and macromolecules arrange themselves laterally or vertically to form a lamellar system [3]. It has long been supposed that the aggregate structure of coal plays a vital role during

coalification [4]. Therefore, it is very necessary to deeply understand the structural evolution mechanism of coal during pyrolysis [5].

In general, the pyrolysis process of coal can be divided into two main stages. One is the depolymerization or decomposition stage where gaseous (e.g., gas and water vapor) and liquid products (e.g., tar) were generated. The other is the condensation or repolymerization stage where the turbostratic lamellar system took place. Amounts of heterogeneous pyrolysis reactions can take place in the aforementioned two types of competitive processes. A better knowledge of coal structure alteration during pyrolysis could promote to comprehend the reaction process of coalification [6, 7]. There have been a number of methods to provide new insights into the relationship between coal structure and its pyrolysis process.

In the past couple of decades, the ex situ XRD and FTIR analytical methods were used widely to supply important information on the changes of coal structure under heat treatment [5, 8, 9]. Mae et al. [10] reported the relationship of the yield of pyrolysis products with coal structure. Wang et al. [11] studied the structure and pyrolysis characteristics of Chinese western coals, demonstrating the relationship between evolution of coal composition and its physicochemical structure. On the basis of X-ray, studies of coal reported by many researchers [12–14] show that the X-ray diffraction pattern of coal resembles a very blurred graphite pattern similar to that obtained with activated carbons and carbon black. Of note, Hirsch [15], Watanabe et al. [16], and Sonibare et al. [17] proposed that the XRD structural parameters (interlayer spacing of crystalline structure (d_{002}) and crystallite sizes (L_a and L_c)) can be used to evaluate the structure of coal and other carbonaceous materials with lower carbon crystallinity. These parameters can be obtained using the Scherrer equation and fitting parameters. For the XRD study of coal structure under pyrolysis conditions, Zhang et al. [18] presented the correlation between coal element composition and coal structure and the evolution of XRD structural parameters of coal with the change of temperature. However, they did not discuss the changes of XRD structural parameters of coal with temperature but also did not study the changes of macromolecular functional groups of coal with temperature, especially oxygen-containing functional groups. Li et al. [19] characterized the structural parameters of coal at different pyrolysis temperatures using in situ XRD technology and obtained the relationship between the corresponding structural parameters and temperature. However, they did not use FTIR technology to analyze the change of functional groups of coal with temperature.

The FTIR technique focuses on determining composition on the physicochemical structures of coal. Kister et al. [20], Christy et al. [21], and Wang et al. [22] obtained that the C=O bonds were almost totally lacking in coal, which had isolated C=C bonds and C≡C bonds, and aliphatic groups CH, CH_2, CH_3, and aromatic ring groups were abundant. Wu et al. [23] used FTIR and TG analysis methods to study the chemical structure evolution and small-molecule gas yield of coal during pyrolysis. However, the FTIR they used is not in situ analysis technology, which is different from this study.

In conclusion, although ex situ analysis technology can also obtain information on coal structure and its reactivity, but because of the complexity of coal structure transformation during pyrolysis, this analysis method cannot characterize the instantaneous information of coal structure at a certain temperature [24]. For that reason, in the present study, the in situ XRD and FTIR analytical techniques were employed at real temperature without cooling coal samples and to assist in quantitative analysis for expounding the structural evolution characteristics of coal during pyrolysis.

The purpose of this study was (1) probing deeply the structural evolution signatures of different ranked coals during pyrolysis using in situ XRD and FTIR analytical techniques; (2) a better understanding of the relationship between the evolution of coal structural parameters and pyrolysis temperature of coal; (3) the reference standard of structure parameters of coal with different ranks under real-time pyrolysis temperature was proposed.

2. Experimental

2.1. Samples and Preparation. A set of five different ranked coals having different geological ages was selected from five coal basins located on North China and South China coal-bearing region (Figure 1). These coal samples were denoted according to their location and geological age as: GZ (Guizhou province, Longtan formation in Late Permian epoch), HB (Hubei province, Chuyanken formation in Late Triassic epoch), HN (Anhui province, Upper Shihezi formation in Late Permian epoch), KL (Hebei province, Lower Shihezi formation in Early Permian epoch), and SX (Shanxi province, Taiyuan formation in Late Carboniferous epoch). Their coal ranks are lignite for SX coal, subbituminous coal for KL coal, bituminous gas coal for HN coal, bituminous coking coal for HB coal, and anthracite for GZ coal in turn.

Each coal sample weighed approximately 200 g. These samples were pulverized and sieved to obtain particles of <56 μm in diameter and dried in a desiccator at 60°C for 12 h. After that, they were demineralized to avoid the interference of mineral matter in coal before subjecting them to in situ XRD and FTIR experiments. Detailed removal process of minerals from coal and preparation of coal KBr pellets were described in previous studies [25].

2.2. Proximate and Ultimate Analyses. The proximate and ultimate analyses of five coal samples before pyrolysis were executed according to ISO 625: 1975 (E) and ISO 333: 1983 (E), respectively. The results are presented in Table 1.

2.3. In Situ FTIR Spectroscopy Measurement. For each set of experiments, after the reactor grasped approximately 20 g coal sample, the reactor was sealed and heated in a temperature-programmed furnace. The heat treatment experiment of coal was carried out under oxygen-free conditions. Five rounds of experiments were conducted at difference temperatures, including 100, 200, 300, 400, and

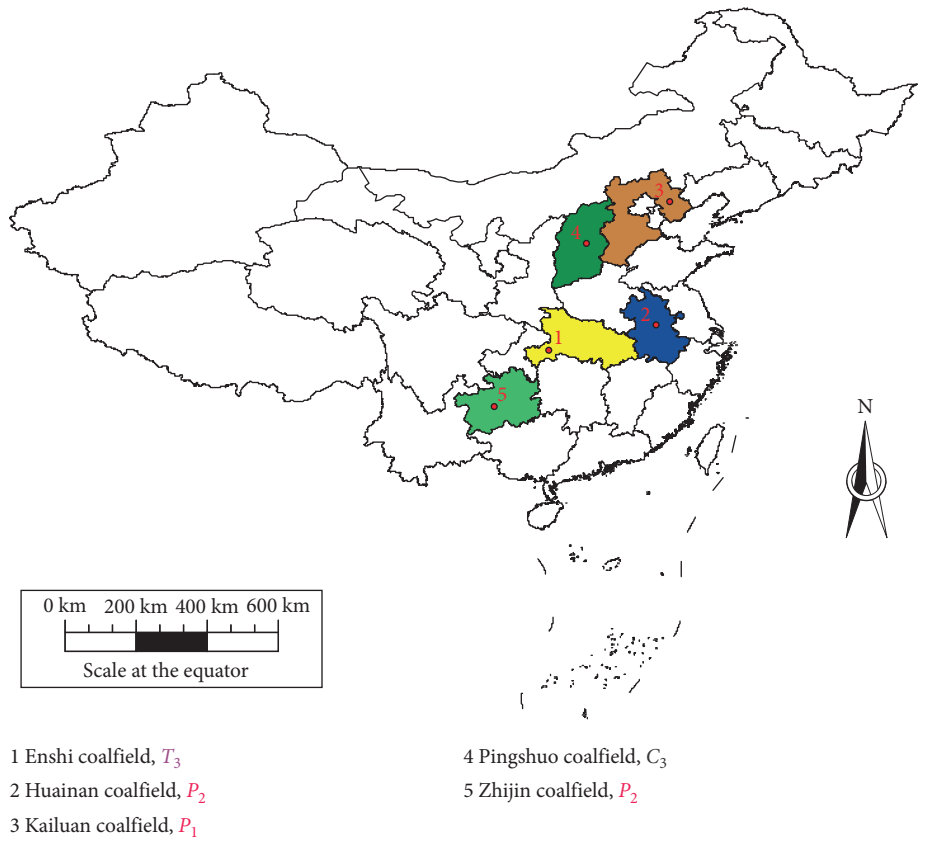

Figure 1: Location and geological ages of Huainan coalfield, Kailuan coalfield, and Pingshuo coalfield in the North China coal-bearing region and Enshi coalfield and Zhijin coalfield in the South China coal-bearing region.

Table 1: Results of proximate and ultimate analyses for five coal samples.

Sample number	Proximate analysis (wt.%)			Ultimate analysis (wt.% daf)					Atomic ratio		O + N + S	Coal rank
	M_{ad}	A_{ad}	V_{daf}	C	H	O	N	S	H/C	O/C		
GZ	1.8	21.3	17.5	91.4	3.1	4.2	0.2	1.0	0.41	0.03	5.4	Anthracite
HB	1.2	12.4	35.0	85.8	5.0	8.1	0.3	0.7	0.70	0.07	9.1	Bituminous coal
HN	1.9	21.6	40.7	80.1	4.5	10.5	1.4	0.3	0.67	0.10	12.2	Bituminous coal
KL	1.2	13.2	33.5	78.5	5.6	13.7	1.2	0.3	0.85	0.13	15.2	Subbituminous coal
SX	2.3	19.9	36.5	71.1	6.1	19.8	1.6	0.4	1.03	0.21	21.8	Lignite

ad: air-dried basis; daf: dried ash-free basis.

500°C. The furnace temperature increased at 5°C/min and was held for 24 hours isothermally after reaching a chosen temperature. Finally, the in situ FTIR spectrograms of coal were measured at each characteristic temperature.

In this work, the infrared spectral bands selected were 2700 to 3000 cm^{-1} and 1300 to 1800 cm^{-1}. In the range of 2700 to 3000 cm^{-1}, two characteristic absorption peaks (2920 and 2860 cm^{-1}) were obtained using fitting parameters. Overlapping peaks in 1300 to 1800 cm^{-1} [25–27] also were separated using the same method. Taking HB as an example, the specific fitting results are exhibited in Figure 2.

The changing features of the infrared spectral structural parameters with respect to different functional groups were previously summarized by José et al. [26]. Nevertheless, the main concern is the influence of heat treatment on the structural parameters of coal in this study. Many spectral parameters based on FTIR have been used to illuminate the structural characteristics of coal [26, 27]. According to the selection of parameters reported in the previous studies, in this study, we focus on the intensity and area ratio of characteristic peaks. The specific parameters and their corresponding functional groups are described as follows:

(i) P_1 and P_2 represent the ratio of the integrated areas of aromatic hydrocarbon CH_x stretching to aliphatic CH_x stretching

(ii) P_3 reveals the variation of oxygen-containing functional groups or the atomic ratio of oxygen to carbon (O/C)

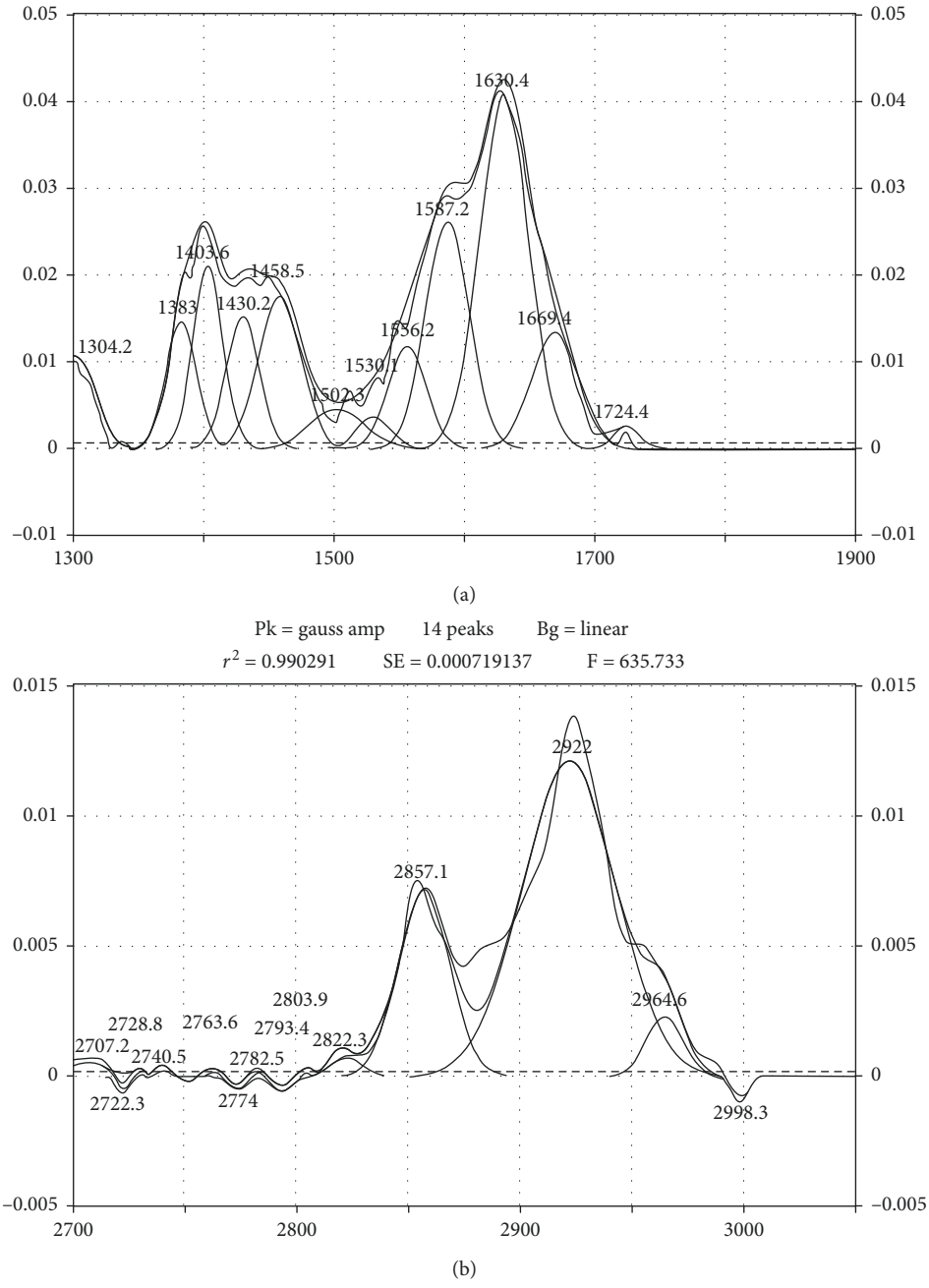

Figure 2: Curve-fitted results of 3000–2800 cm^{-1} and 1300–1800 cm^{-1} band for HB coal sample before pyrolysis.

(iii) P_4 and P_5 estimate the degree of enrichment of CH_3 from residual aliphatic structures

2.4. In Situ X-Ray Diffraction Measurement. The in situ XRD data collection was performed by Philips X'Pert PRO X-ray powder diffraction, using Ni-filtered Cu Kα radiation and a scintillation detector. The XRD pattern was recorded over a 2θ interval of 10–60°, with a step size of 0.034 and 2 s/step counter time. The heat treatment experiment of coal was carried out under oxygen-free conditions. Five powered coal samples were heated from room temperature to 900°C with the heating rate of 10°C/min and were kept at constant temperature (25, 100, 200, 300, 400, 500, 600, 700, 800, and 900°C) for 20 min. Meanwhile, the in situ XRD diffractograms were monitored at each characteristic temperature. Structural parameters (L_a, L_c, and d_{002}) were calculated according to Scherrer equations (1)–(3), respectively:

$$\text{crystalline lateral size: } L_a = \frac{1.84\lambda}{B_{100}\cos(\varphi_{100})}, \quad (1)$$

$$\text{stacking height: } L_c = \frac{0.89\lambda}{B_{002}\cos(\varphi_{002})}, \quad (2)$$

$$\text{interlayer spacing: } d_{002} = \frac{\lambda}{2\sin(\theta_{002})}, \quad (3)$$

where λ refers to the wavelength of the radiation in the experiment (λ is 1.5406 Å in this study). B_{100} and B_{002} represent the width of (100) and (002) peaks at half-maximum height, respectively. φ_{100} and φ_{002} represent the peak position of (100) and (002) peaks, respectively. The θ_{002} refers to the Bragg angle of (002) peak.

3. Results and Discussion

3.1. Relationship between Coal Element Composition and Its Structure. Some information about the molecular structures of coal can be obtained from an analysis for the elements carbon (C), hydrogen (H), sulfur (S), and nitrogen (N) [28]. The atomic ratio of hydrogen to carbon (H/C) varies in different ranked coals. From Table 1, it is seen that lignite (SX), subbituminous coal (KL), and bituminous coals (HB and HN) have higher H/C ratios (from 1.03 to 0.70), whereas anthracite (GZ) has the lowest H/C ratio (0.41). The results show the H/C ratio decreases with the degree of coalification. Furthermore, the total content of O + N + S in coal differs appreciably. With the increase of coal rank, the O + N + S content in coal decreases significantly (Table 1), because the O, N, and S would be taken off during coalification, finally forming a graphite-like structure which would have a lower atomic H/C ratio. According to Hirsch [29], in this study, SX and KL, and HN coals (<85% C_{daf}) have an "open" structure with lamellae rarely oriented and connected by cross-links, and HB coal (85% < $C_{daf} \leq$ 91%) has a "liquid" structure with lamellae some oriented and many cross-links interrupted, and GZ coal (>91% C_{daf}) has an "anthracitic" structure with both lamellae and pores orientated.

3.2. FTIR Investigation

3.2.1. FTIR Characteristics of Coal before Pyrolysis. The infrared spectra of coal with the increase of coal rank are shown in Figure 3. Assignments of characteristic peak positions corresponding to different functional groups are also depicted in Figure 3 based on [26, 30–33]. As shown in Figure 3, the regular change of infrared characteristic peak of coal was closely related to the increase of C_{daf} content in coal. According to Van Krevelen [34], the absorbance of functional groups decreases considerably depending on the degree of coalification.

The following conclusions can be drawn in the coal series lignite-subbituminous coal-bituminous coal-anthracite based on Figure 3:

(1) The dashed line 2 between 2850 cm^{-1} and 3000 cm^{-1} reveals that, with the increase of coal rank, the absorbance of aliphatic CH_2 or CH_3 stretching vibration dwindles considerably, suggesting the decrease of hydrocarbon content in coal. The change in dashed 1 (aromatic hydrocarbon) was similar to that in dashed line 2, which indicates that hydrogen was gradually removed in higher-rank coal, leading to the decrease of intensity of aromatic ring stretching vibration in coal.

(2) In lignite (SX) and subbituminous coal (KL), the absorbance of aromatic carboxyl and carbonyl groups (dashed line 3) was obvious. However, it was absent in bituminous coal (KL and HN) and anthracite (GZ). According to Van Krevelen [34], it can be deduced that as coal rank increases, most of the carboxyl and carbonyl groups in coal can be gradually incorporated into the orthoquinone system structure.

(3) Because of the presence of polar substituents in aromatic rings [30, 31], the absorbance of aromatic nucleus C=C groups (dashed line 4) starts to decrease from lignite (SX) to bituminous coal (HN) and then increases from bituminous coal (HB) to anthracite (GZ).

(4) In the range of lignite (SX) to bituminous coal (HN), the absorbance of phenolic deformation C–O–C groups (dashed line 5) decreases obviously. Up to anthracite (GZ), it disappears progressively.

(5) The absorbance of aromatic out-of-plane bending (dashed line 6) increases slightly between lignite (SX) and subbituminous coal (KL). Reaching the stage of bituminous coal (HB), it decreases moderately. Up to anthracite (GZ), it decreases to a less content.

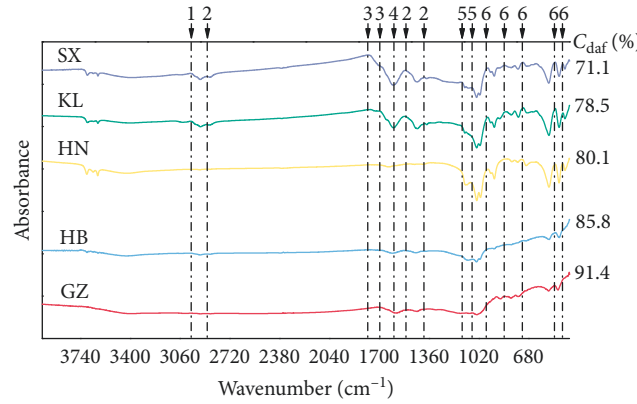

Figure 3: Infrared spectrogram of five coal samples. Attribution of characteristic peak positions is descried as follows: (1) aromatic hydrocarbon CH; (2) aliphatic CH_2 or CH_3 stretching vibration; (3) aromatic carbonyl/carboxyl groups (C=O); (4) aromatic nucleus (C=C); (5) phenolic deformation C–O–C (stretching); (6) aromatic CH (out-plane bending).

3.2.2. In Situ FTIR Evolution Characteristics of Different Rank Coals during Pyrolysis. As the pyrolysis temperature increases, in situ infrared spectra of five coal samples are shown in Figure 4. In the range of 3800 to 3200 cm^{-1}, this absorption band is assigned to the –OH groups, which stands for the presence of phenols, ethers, and alcohols.

According to Sonibare et al. [17], this absorption band can also reflect the vibration intensity of water molecules in coal. In comparison to low-ranked coal (Figures 4(a)–4(c)),

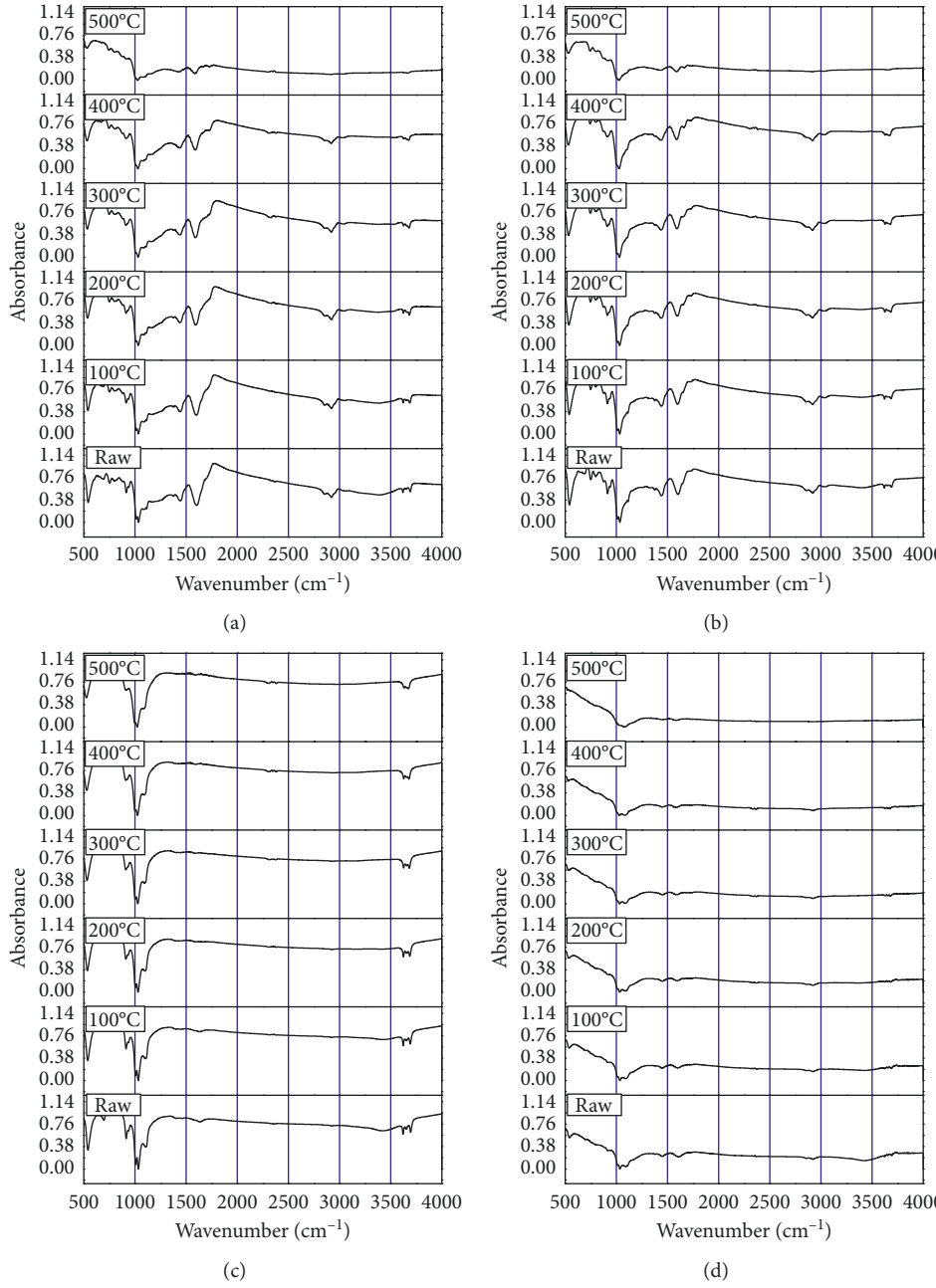

Figure 4: Continued.

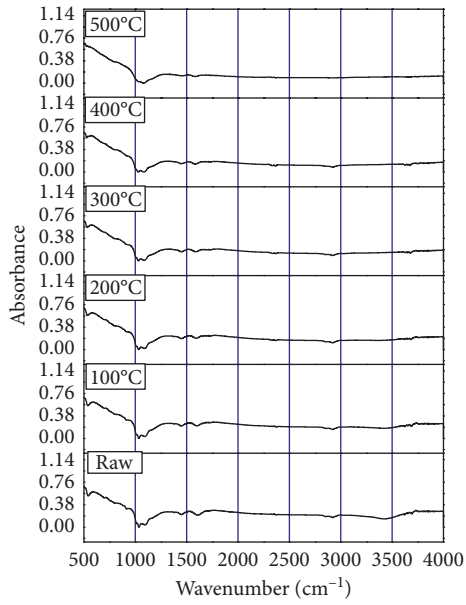

Figure 4: In situ infrared spectra of five coal samples at different temperatures: (a) SX; (b) KL; (c) HN; (d) HB; (e) GZ.

it can be clearly observed that the absorbance of this characteristic band disappeared almost in anthracite (Figures 4(d) and 4(e)), suggesting that the high-ranked coal contains no intrinsic water molecules. Only lignite (SX) and subbituminous coal (KL) between 3000 cm^{-1} and 2800 cm^{-1} reflects strong absorption peaks at 2920 and 2850 cm^{-1}, representing aliphatic and aromatic stretching vibration including $-CH_2$ and $-CH_3$. However, in bituminous coal (HN and HB) and anthracite (GZ), this characteristic band has no response. Lignite (SX) also presents a characteristic band at approximately 1440 cm^{-1}, corresponding to aliphatic C=C bending vibration. Noteworthy, a characteristic band at approximately 610 cm^{-1} appears in all coal samples. It was attributed to the C–S stretching vibration based on the study by Angoni [13] and Sonibare et al. [17]. Likewise, some peaks between 900 cm^{-1} and 700 cm^{-1} ascribed to the existence of low intensity aromatic $(C–H)_{ar}$ and its out-of-plane bending modes are also present in all coal samples. This result means that the existence of this characteristics band was independent on the increase of coal rank.

Especially, significant changes in the oxygen-containing functional groups are observed in the range of 1600 to 1800 cm^{-1} band (Figure 4). The curve-fitting results (Figure 2) reveal the presence of three characteristics peaks at approximately 1724, 1669, and 1630 cm^{-1}, which were attributed to phenolic esters, carboxylic acids, and conjugate ketonic structures, respectively [35]. Given that the importance of this band, we examine the changes in oxygen-containing functional groups from two perspectives.

(1) Effect of Temperature on Oxygen-Containing Functional Groups. For lignite-subbituminous coal-bituminous coal-anthracite series, with the increase of temperature from 100 to 500°C, the absorption at ~1724 cm^{-1} shifts to ~1694 cm^{-1} because the vibration intensity of aliphatic esters and phenol esters was reduced [34, 35]; the band of carboxylic acids shifts from ~1669 cm^{-1} to ~1644 cm^{-1}, which reflects a progressive conversion of aliphatic carboxylic acids into aromatic carboxyls [35]; the slight excursion of conjugated structures was detected from ~1630 to ~1620 cm^{-1}. On the other hand, the intensity of the above characteristic band decreases slightly from 100 to 400°C and drops abruptly at 500°C. More generally, coal pyrolysis can be divided into a three-step process associated with different chemical reactions that take place in three temperature range intervals, <300, 300–600, and 600–800°C. According to Arenillas et al. [30, 31], the pyrolysis process of coal in the corresponding temperature ranges can be described as follows: (1) degassing; (2) depolymerization; (3) polycondensation. The full pyrolysis of coal usually takes place in "depolymerization." Based on this, it can be deemed that when the temperature was higher than 400°C, the studied coal began to "depolymerize," leading to the decomposition of the relatively high molecular weight substances [30, 31].

(2) Effect of Coal Rank at the Same Temperature on Oxygen-Containing Functional Groups. Figure 5 shows in situ infrared spectra of five coal samples at the same temperature. As can be seen from Figure 5, under the same temperature conditions, in the range of lignite (SX) to bituminous coal (HN), the absorbance of carboxyl groups at ~1700 cm^{-1} and phenolic ester groups at ~1500 cm^{-1} decreases slightly. These two characteristic bands between bituminous coal (HB) and anthracite (GZ) almost disappear. The result shows that as the coal rank increases, the intensity of decarboxylation and decarbonylation becomes deeper correspondingly [30–32]. Interestingly, once the temperature reaches 500°C, their absorbance can drop immediately, which indicates that the

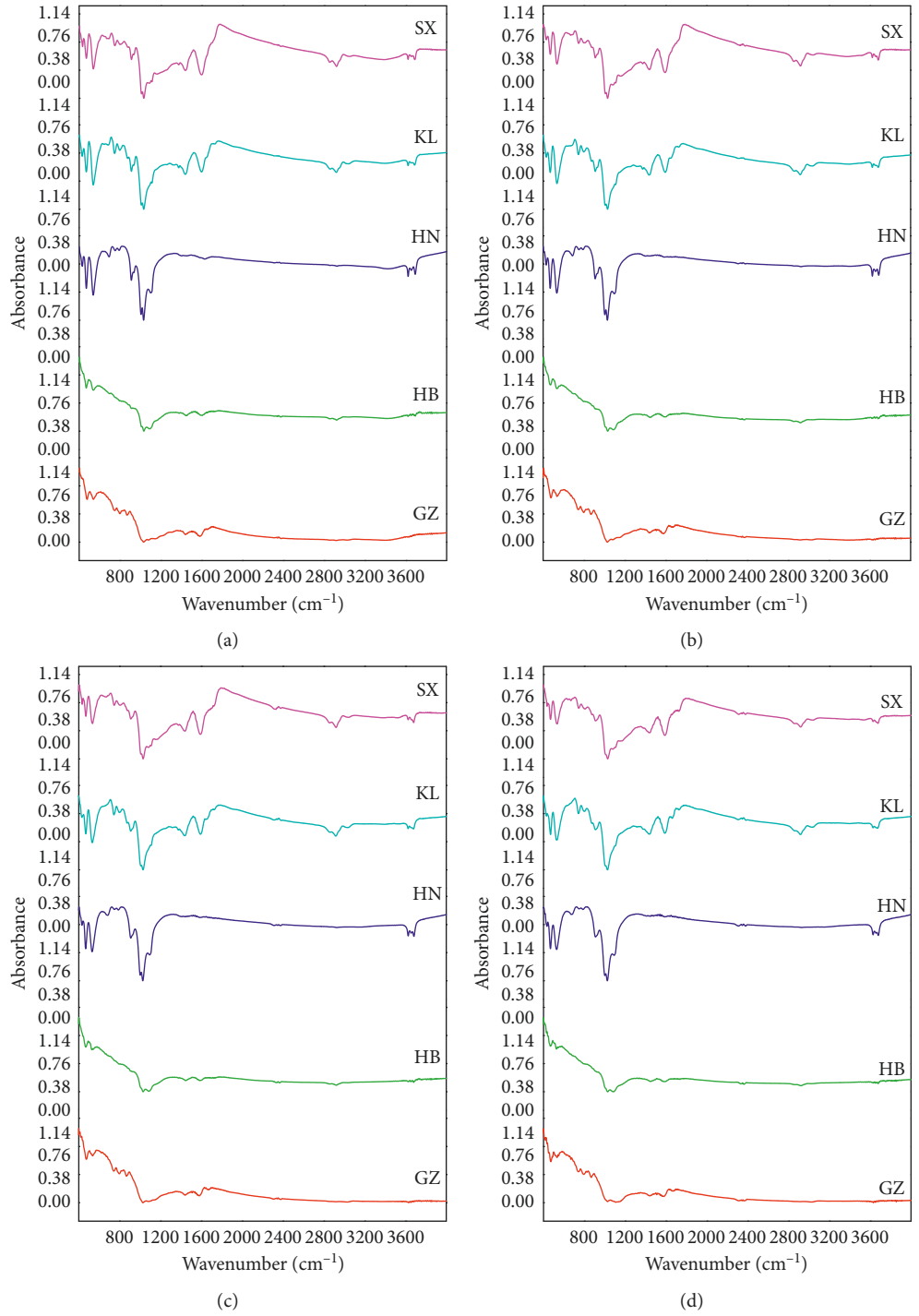

Figure 5: Continued.

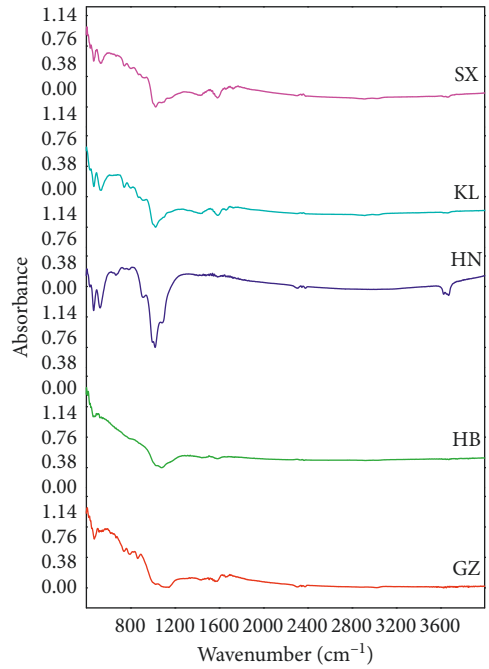

Figure 5: In situ infrared spectra of five coal samples at the same temperature: (a) 100°C; (b) 200°C; (c) 300°C; (d) 400°C; (e) 500°C.

degree of coal pyrolysis is not related to the degree of coalification and may be related to the bond energy of covalent bond of oxygen-containing groups in coal [33].

3.2.3. Effect of Temperature on Structural Parameters. The calculated infrared spectral structural parameters are presented in Table 2. For raw coal, with the increase of coal rank, the structural parameters (P_1, P_2, P_3, P_4, and P_5) of coal increase accordingly, which means that high-ranked coal (GZ and HB) containing less H, less O, and more C becomes more aromatic than lower-ranked coal (HN, KL and SX). However, these parameters change in a different way after coal pyrolysis. The detailed conclusions can be drawn as follows:

(1) For these samples (GZ, HB, and HN), the contraction vibration intensity of the $-CH_3$ band (2920 cm^{-1} and 2860 cm^{-1}) is very weak at different temperatures and the peak area of this band cannot be obtained so that the P_1 value cannot be calculated. For KL and SX samples, the P_1 value shows a decreasing trend with the increase of temperature at less than 500°C. Above 500°C, the P_1 value cannot be calculated. This indicates that the absorption peaks of hydrogen on aliphatic hydrocarbon and naphthenic hydrocarbon groups appear at 2920 cm^{-1} and 2860 cm^{-1}, and the absorption intensity of these peaks decreases significantly with the deepening of the coalification degree (after KL coal). For low-rank coals (KL and SX), the intensity of these peaks also decreased significantly when the temperature exceeded 400°C; (2) with the increase of coal rank, the P_2 value of coal tends to increase to a certain extent. However, for the same coal sample, with increasing temperature, the P_2 value of coal gradually decreases. This indicates that temperature changes the molecular structure of coal and weakens the absorption of hydrogen on aliphatic and aromatic hydrocarbon groups; (3) with the increase of coal rank, P_3 value shows a certain increasing trend. For low-rank coal, there is a strong absorption peak at 1600 cm^{-1}, while for high-rank coal, the intensity of the absorption peak decreases. This absorption peak may be attributed to the overlap of hydrogen-bonded carbonyl group and aromatic ring C=C double bond absorption, which gradually weakens with the deepening of coalification. By analyzing the infrared spectrum of coal, it can be seen that the attenuation of 1600 cm^{-1} absorption peak is higher than that of 1700 cm^{-1}, so P3 value increases. Moreover, the reduction of P_3 value during coal pyrolysis shows that, with the increase of polymerization and decrease in the atomic O/C ratio, the amount of oxygen-containing functional groups in coal starts to decrease progressively; (4) P_4 and P_5 are both ratios reflecting the intensity of hydrogen absorption peaks on aliphatic and aromatic hydrocarbon groups. With the increase of coal rank, they all show different degrees of increase. For the same coal sample, as the temperature increases, they also gradually increase. This reflects that temperature increases the vibration intensity of aromatic and aliphatic CH_x groups, resulting in an increase in the number of some oxygen-containing functional groups in coal.

3.3. XRD Investigation

3.3.1. XRD Characteristics of Coal before Pyrolysis. More generally, coal is amorphous, but its aromatic structure tends to graphitize gradually during coalification. Thus, the XRD

Table 2: Statistic results of the infrared spectral structural parameters of five coal samples before and after pyrolysis.

Sample number	Temperature (°C)	Structural parameters				
		P_1	P_2	P_3	P_4	P_5
GZ	Raw coal	–	1.965	0.885	1.062	0.585
	100°C	–	1.941	0.880	1.063	0.592
	200°C	–	1.894	0.867	1.066	0.599
	300°C	–	1.817	0.842	1.072	0.606
	400°C	–	1.693	0.794	1.087	0.612
	500°C	–	1.492	0.699	1.127	0.619
HB	Raw coal	–	1.843	0.830	0.997	0.546
	100°C	–	1.821	0.825	0.997	0.552
	200°C	–	1.777	0.813	1.000	0.559
	300°C	–	1.705	0.790	1.005	0.565
	400°C	–	1.588	0.745	1.020	0.572
	500°C	–	1.399	0.656	1.057	0.578
HN	Raw coal	–	1.766	0.812	0.954	0.541
	100°C	–	1.721	0.776	0.931	0.555
	200°C	–	1.701	0.771	0.932	0.562
	300°C	–	1.660	0.760	0.934	0.568
	400°C	–	1.592	0.738	0.939	0.575
	500°C	–	1.483	0.695	0.953	0.581
KL	Raw coal	2.947	1.687	0.760	0.912	0.502
	100°C	2.916	1.667	0.756	0.913	0.508
	200°C	2.852	1.626	0.745	0.915	0.514
	300°C	2.743	1.561	0.723	0.920	0.520
	400°C	2.559	1.454	0.682	0.934	0.526
	500°C	–	1.281	0.600	0.968	0.532
SX	Raw coal	2.668	1.528	0.688	0.826	0.455
	100°C	2.641	1.510	0.684	0.827	0.461
	200°C	2.583	1.473	0.674	0.829	0.466
	300°C	2.484	1.413	0.655	0.833	0.472
	400°C	2.317	1.316	0.617	0.845	0.477
	500°C	–	1.160	0.543	0.877	0.483

The parameter calculation method: $P_1 = \text{area}_{2920+2860\,\text{cm}^{-1}}/\text{area}_{1600\,\text{cm}^{-1}}$; $P_2 = \text{area}_{1380+1460\,\text{cm}^{-1}}/\text{area}_{1600\,\text{cm}^{-1}}$; $P_3 = \text{area}_{1700\,\text{cm}^{-1}}/\text{area}_{1600\,\text{cm}^{-1}}$; $P_4 = \text{area}_{1380\,\text{cm}^{-1}}/\text{area}_{1460\,\text{cm}^{-1}}$; $P_5 = \text{area}_{1380\,\text{cm}^{-1}}/\text{area}_{2920\,\text{cm}^{-1}}$.

pattern of coal presents certain regularity with the increase of the degree of coalification.

Figure 6(a) is an XRD pattern of five coal samples before pyrolysis using the Debye–Scherrer method [28], with coal rank increasing sequentially from top to bottom. It can be seen from the diffraction pattern that anthracite (GZ) has the uppermost diffraction peak (002) and the narrowest width (002). The diffraction width and height of bituminous coal (HB and HN) and subbituminous coal (KL) are similar, but both are lower and wider than those of anthracite. Compared with other coals, the diffraction height and width of lignite (SX) are the lowest and widest. The shape change of diffraction curves of five coal samples has certain regularity. With increasing coal rank, the diffraction height on the diffraction curves also increases correspondingly, while the diffraction width becomes narrow progressively, and the diffraction position shifts gradually to the high angle ($2\sin\theta/\lambda$) region. Taking the 2θ angle values corresponding to (002) crystal mesh of five coal samples as an example, this change can be clearly observed (Table 3) that the position of (002) band shifts gradually to a high angle value ($2\sin\theta/\lambda$) from 0.27 to 0.29.

As shown in Figure 6(a), the asymmetric phenomenon of the (002) band suggests the existence of another band (λ) at its left-hand side, which makes the left side of the (002) band broad and diffused [25]. The diffraction height of the (λ) band at low angle becomes relatively higher due to strong scattering between low-angle particles. As coal rank increases, the height of the (002) band becomes higher but the height of the (λ) band becomes lower.

Taking the SX coal sample as an example, its XRD pattern was fitted using Gaussian function (Figure 6(b)). In conjunction with Scherrer equations (1)–(3), the XRD structural parameters of five coal samples were calculated and are presented in Table 3.

Table 3 shows that the interlayer spacing of carbon hexagons (d_{002}) is 0.3567 nm in lignite (SX), 0.3571 nm in subbituminous coal (KL), 0.3561 nm in bituminous gas coal (HN), 0.3518 nm in bituminous coal (HB), and 0.3498 nm in anthracite (GZ). The results show with the increase of coal rank, the d_{002} values decreases accordingly. Compared with the d_{002} value (0.335 nm) of graphite, the d_{002} values of five coal samples were significantly greater, which suggests a lower degree of the crystalline order in these coals. From Table 3, the crystallite height (L_c) value increases from 1.379 nm for lignite (SX) to 1.984 nm for anthracite (GZ), but the crystallite diameter (L_a) value shows the different trend relative to L_c. In all coal samples, the L_a remains

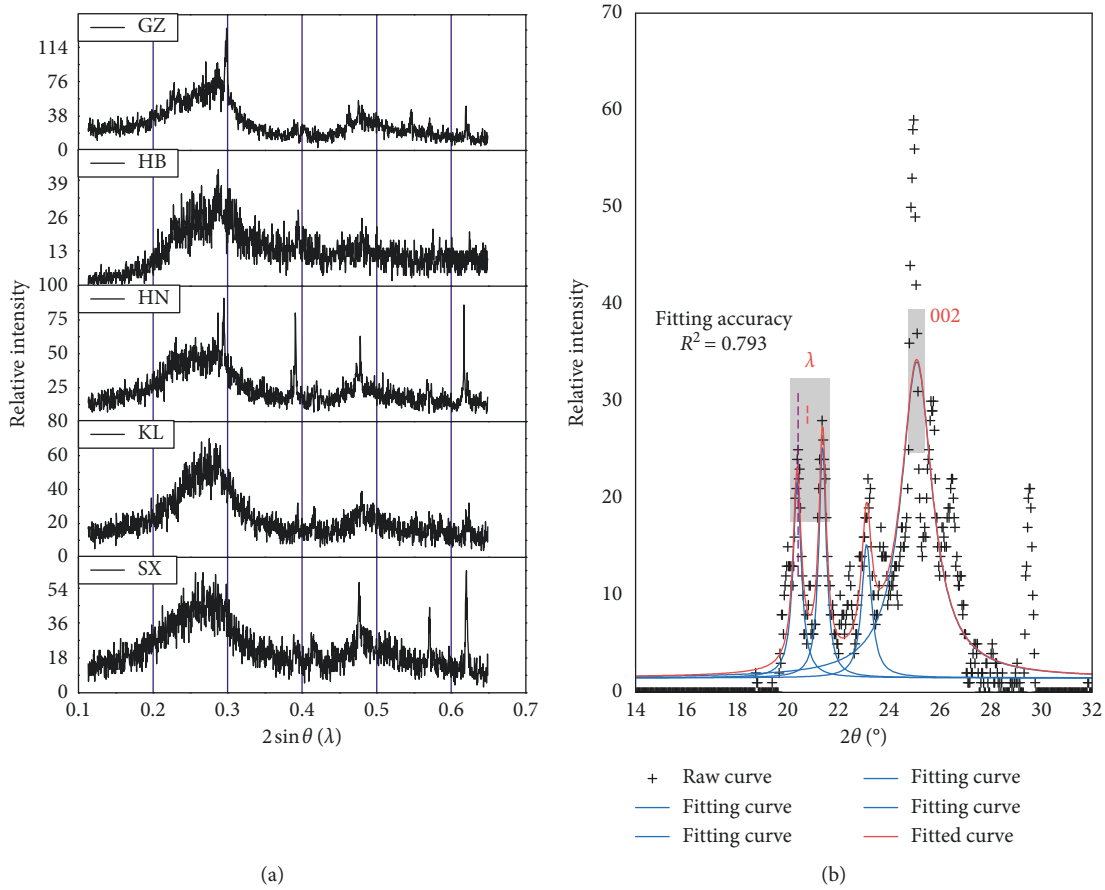

FIGURE 6: XRD pattern of five coal samples before pyrolysis (a) and the curve fitting result of the SX coal sample before pyrolysis as a function of Gaussian function (b).

constant at nearly 2.979 nm. The same conclusion was also documented in the literature [36]. It can be deemed that with increasing coal rank, the degree of polymerization between adjacent carbon crystals was restricted by molecular forces between side chains [36]. Combining L_a and L_c changes, it can be speculated that the natural orientation under pressure and geothermal gradient can be direction-dependent during coalification [8].

3.3.2. In Situ XRD Evolution Characteristics of Different Coals during Pyrolysis. The in situ XRD patterns of five coal samples during pyrolysis are shown in Figure 7.

As can be seen from Figure 7, the shape of the XRD pattern of five coal samples did not change significantly before 500°C. In comparison to coal before pyrolysis, the XRD patterns of all coals present a more sharp band (λ) at approximately 0.23 ($2\sin\theta/\lambda$) in the range of 25 to 500°C. When temperature is up to 900°C, the intensity of the (λ) band decreases significantly. On the other hand, the position of the (002) band remains unchanged firstly between 25°C and 500°C, but above 500°C, the shape of the (002) band becomes sharper and shifts to higher 2θ angle values. In addition, this band tends to be more asymmetric above 500°C than at lower temperatures (Figures 7(c)–7(e)).

3.3.3. Effect of Temperature on Structural Parameters. Taking the HB coal sample as example, Origin 8.0 software was used to fit its XRD patterns in the 2θ range of 14–32° to obtain (002) and (λ) bands and their structural parameters (d_{002}, L_a, and L_c). The in situ XRD curve fitting results of the HB coal sample at different temperatures (300, 600, and 900°C) are shown in Figure 8.

Table 3 shows in situ XRD structural parameters of five coal samples at different temperatures. Figure 9 plots the correlation between temperature and the above structural parameters. Some conclusions were obtained as follows:

(1) L_a. Figure 9(a) shows that, with increasing temperature, the variation range of L_a value is extremely small (approximately 0.09 nm), suggesting that the relationship between the L_a value of coal and temperature becomes quite inappropriate. According to Hirsch [29] and Lu et al. [36], it can be deemed that, with increasing temperature, the bridge structure in coal becomes unstable as a reaction to increasing forces in the aromatic nucleus but this structure may differ in molecular weight and may contain several types of geometric and positional isomers. As a result, the change of L_a for aromatic nucleus is complexity and heterogeneity. In this study, the variation of L_a value is in accordance with the reported in the literature [8, 36].

Table 3: Statistic results of the XRD parameters of five coal samples before and after pyrolysis.

Sample number	Temperature (°C)	▲ (°)		▼ (nm)		
		$2\theta_{002}$	$2\theta_{100}$	d_{002}	L_c	L_a
GZ	Raw coal	26.15	46.16	0.3498	1.9841	3.0507
	25°C	26.17	44.64	0.3496	1.9848	2.9172
	100°C	26.26	45.93	0.3485	1.9842	3.0073
	200°C	26.21	45.09	0.3491	1.9842	2.9479
	300°C	26.27	45.28	0.3483	1.9842	2.9611
	400°C	26.26	44.38	0.3485	1.9837	2.8998
	500°C	26.24	44.14	0.3487	1.9833	2.8839
	600°C	26.35	44.61	0.3474	1.9868	2.9152
	700°C	26.40	45.30	0.3468	1.9876	2.9625
	800°C	26.54	45.02	0.3451	1.9897	2.9431
	900°C	26.59	45.51	0.3444	1.9901	2.9773
HB	Raw coal	25.99	45.38	0.3518	1.8797	2.9681
	25°C	26.04	45.26	0.3512	1.8801	2.9598
	100°C	26.00	45.53	0.3516	1.8796	2.9787
	200°C	26.00	45.25	0.3516	1.8792	2.9591
	300°C	26.00	45.26	0.3517	1.8805	2.9598
	400°C	25.96	45.16	0.3521	1.8781	2.9528
	500°C	25.93	45.60	0.3525	1.8793	2.9837
	600°C	26.19	45.53	0.3493	1.8826	2.9787
	700°C	26.25	44.98	0.3486	1.8828	2.9404
	800°C	26.40	45.12	0.3468	1.8866	2.9500
	900°C	26.43	44.96	0.3464	1.8868	2.9390
HN	Raw coal	25.66	45.72	0.3561	1.6786	2.9922
	25°C	25.69	45.87	0.3557	1.6796	3.0030
	100°C	25.65	45.66	0.3562	1.6786	2.9879
	200°C	25.61	45.76	0.3567	1.6772	2.9951
	300°C	25.72	45.01	0.3553	1.6781	2.9424
	400°C	25.54	45.57	0.3576	1.6816	2.9815
	500°C	25.63	46.72	0.3565	1.6806	3.0656
	600°C	25.88	46.64	0.3532	1.6852	3.0596
	700°C	25.89	45.87	0.3531	1.6847	3.0030
	800°C	26.17	45.60	0.3496	1.6885	2.9837
	900°C	26.19	45.66	0.3493	1.6882	2.9879
KL	Raw coal	25.58	45.56	0.3571	1.5786	2.9808
	25°C	25.65	45.64	0.3562	1.5796	2.9865
	100°C	25.58	46.20	0.3571	1.5786	3.0270
	200°C	25.47	45.31	0.3585	1.5772	2.9632
	300°C	25.54	46.55	0.3576	1.5781	3.0529
	400°C	25.80	45.36	0.3543	1.5816	2.9667
	500°C	25.73	45.36	0.3552	1.5806	2.9667
	600°C	26.07	46.60	0.3509	1.5852	3.0566
	700°C	26.03	46.20	0.3513	1.5847	3.0270
	800°C	26.31	45.59	0.3479	1.5885	2.9830
	900°C	26.29	45.70	0.3481	1.5882	2.9908
SX	Raw coal	25.61	45.43	0.3567	1.3791	2.9717
	25°C	25.61	44.61	0.3567	1.3791	2.9152
	100°C	25.54	46.54	0.3576	1.3781	3.0521
	200°C	25.54	45.31	0.3576	1.3781	2.9632
	300°C	25.54	45.66	0.3576	1.3781	2.9879
	400°C	25.47	45.30	0.3585	1.3772	2.9625
	500°C	25.42	44.78	0.3592	1.3765	2.9267
	600°C	25.64	46.01	0.3563	1.3794	3.0131
	700°C	25.76	45.71	0.3548	1.3812	2.9915
	800°C	25.88	43.53	0.3532	1.3826	2.8444
	900°C	25.92	44.67	0.3527	1.3832	2.9192

▲: characteristic parameters of diffraction peak. ▼: crystallite structure parameters.

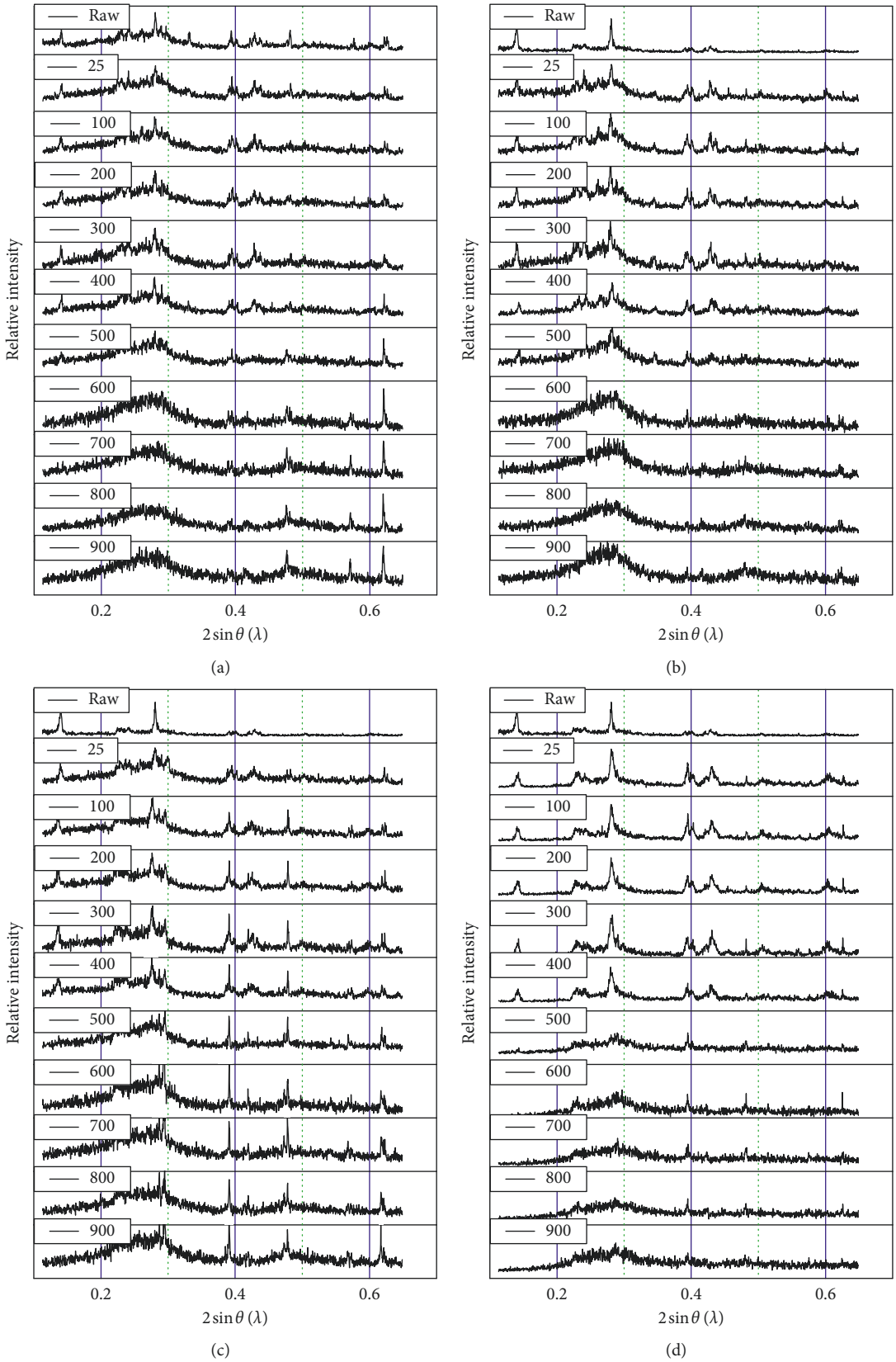

Figure 7: Continued.

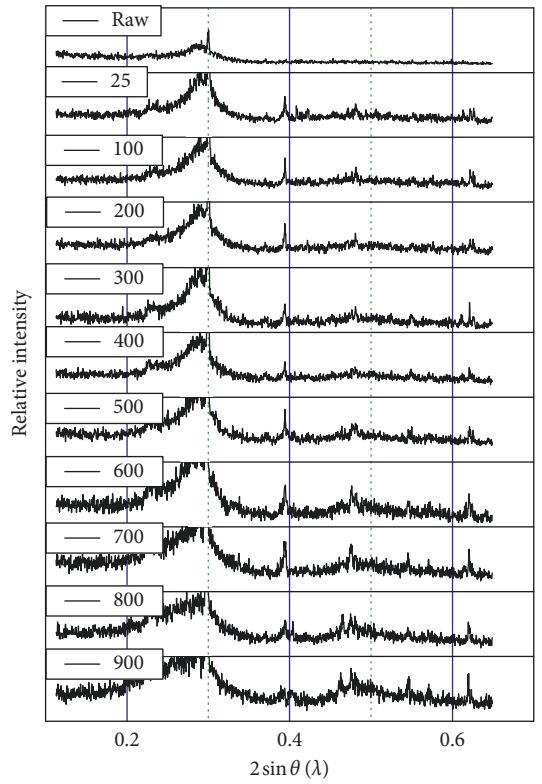

(e)

Figure 7: In situ XRD pattern of five coal samples at different temperatures: (a) SX; (b) KL; (c) HN; (d) HB; (e) GZ.

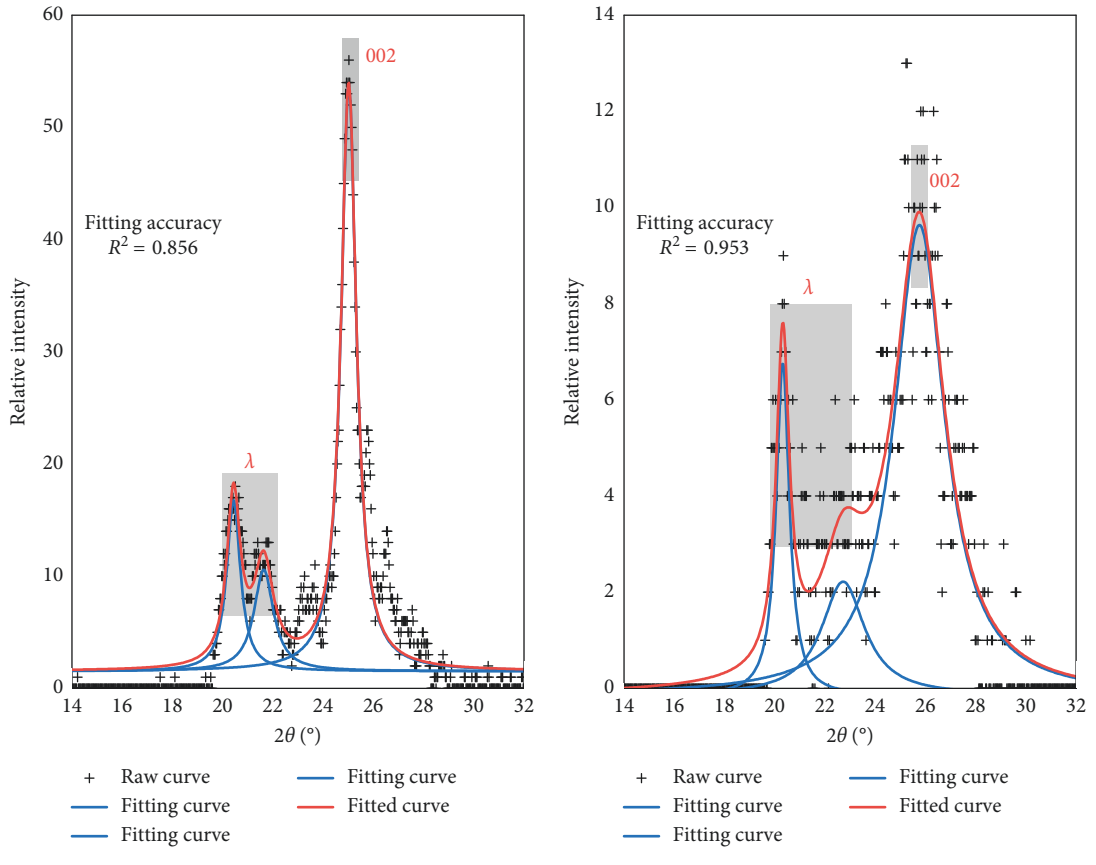

(a) (b)

Figure 8: Continued.

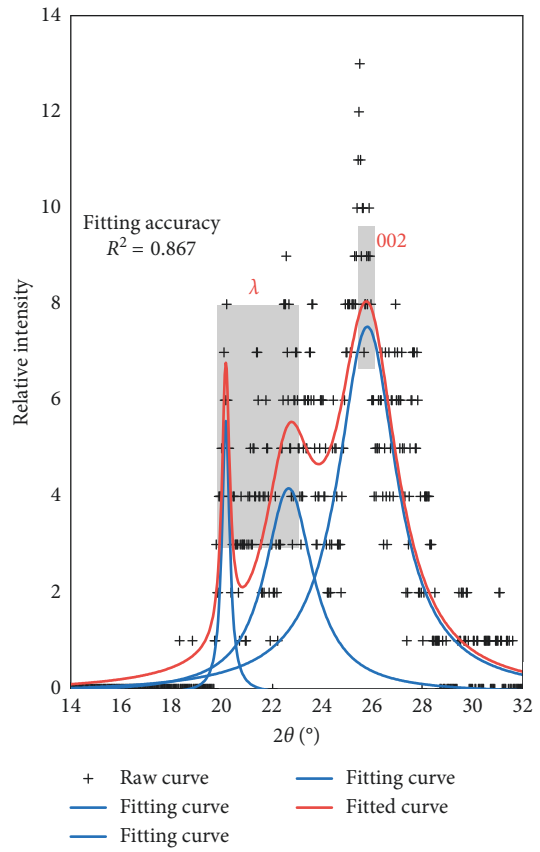

Figure 8: In situ XRD curve fitting results of the HB coal sample at different temperatures: (a) 300°C; (b) 600°C; (c) 900°C.

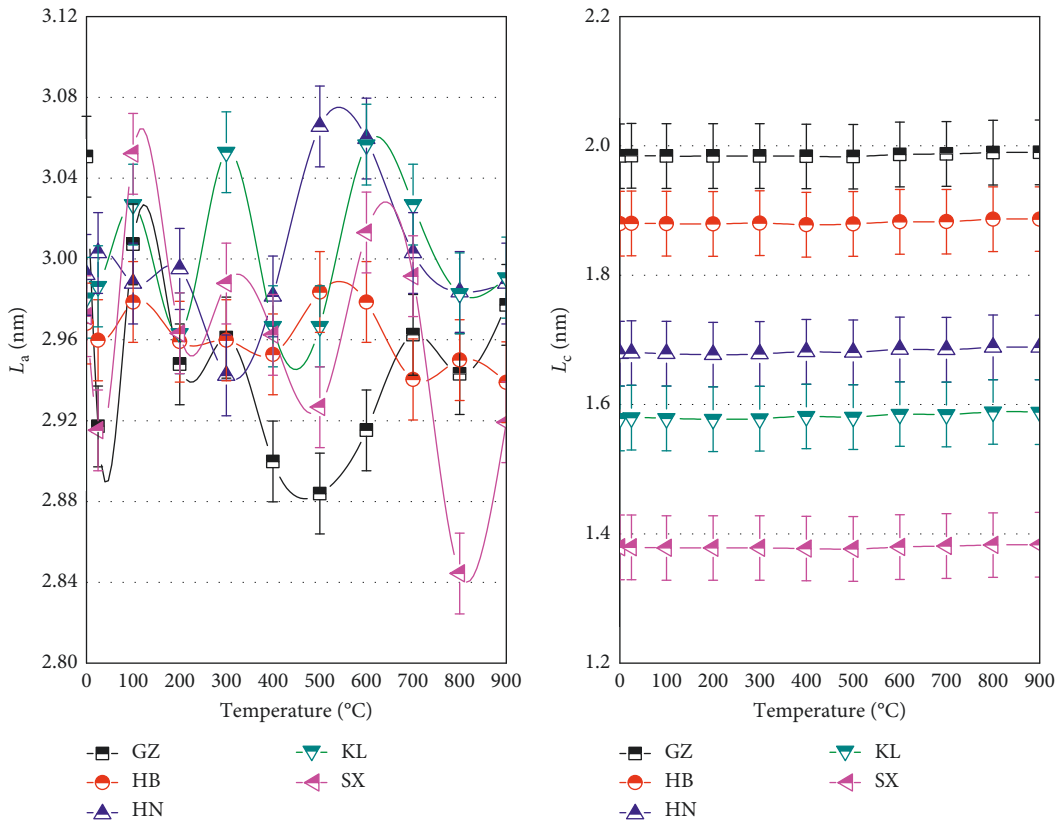

Figure 9: Continued.

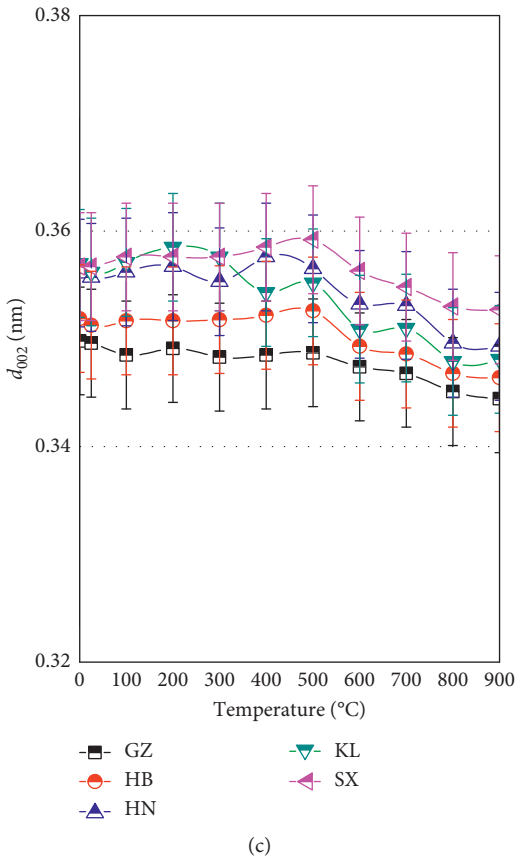

Figure 9: Variation of XRD structural parameters with temperature.

(2) L_c. Figure 9(b) shows that, with increasing temperature, the change trend of L_c value can be divided into two main stages. There is a slight decline in the range of 25 to 500°C. After 500°C, the L_c shows a degree of increase. This phenomenon is likely to be related to an evident change in the structure caused by the expulsion of hydrocarbons and other gases physically trapped in the inertinite network [30].

(3) d_{002}. The d_{002} that is considered to be a measure of the perfection in the two-dimensional turbostratic system is characteristic of the substances with two-dimensional periodicity [29]. Figure 9(c) shows that, with increasing temperature, the change of d_{002} values reflects two different changing processes. One stage is in the range of 25–500°C. In this stage, the aggregate d_{002} value increases obviously in lignite (SX) and bituminous coal (HN and HB), whereas it decreases slightly in anthracite (GZ). The other stage is between 500°C and 900°C, where the d_{002} value decreases considerably. This is a good evidence to demonstrate positively such change dependence on the increase of temperature rather than coal rank.

4. Conclusions

The structural evolution signatures of different ranked coal during pyrolysis were deeply investigated using in situ XRD and FTIR analytical methods. The main conclusions are as follows: (1) the FTIR spectra analysis shows that when temperature reaches between 400 and 500°C, coal structure occurs in abrupt change in the intensity of absorption peak; (2) the X-ray diffraction analysis illustrates that with the increase of temperature, two parameters (d_{002} and L_c) change accordingly, but the value of L_a remains unchanged; (3) combining the results of the two experiments, it can be seen that, in the temperature range of less than 500°C, the size of aromatic lamellae of coal decreases, the distance between lamellae decreases, and the degree of bridge bond breaking, aliphatic side chain cracking, and oxygen-containing functional group cracking rises, suggesting that the degree of aromatization of coal increase.

Data Availability

In this study, the data form mainly includes (1) original spectral data (XRD and FTIR) and (2) spectral parameters. The original spectral data used to support the findings of this study are available from the corresponding author upon request. The spectral parameters data used to support the findings of this study are included within the article.

Conflicts of Interest

The authors declare that there are no conflicts of interest regarding the publication of this paper.

Acknowledgments

We acknowledge support from the Research Projects of Department of Land and Resources of Anhui Province, China (2016-K-2), National Natural Science Foundation of China (No. 41502152), Open Projects of Research Center of Coal Resources Safe Mining and Clean Utilization, Liaoning (LNTU17KF10), Natural Science Foundation General Program of Anhui Program (1808085MA07), and Natural Science Foundation Youth Program of Anhui Program (1808085QE150).

References

[1] B. Feng, S. K. Bhatia, and J. C. Barry, "Structural ordering of coal char during heat treatment and its impact on reactivity," *Carbon*, vol. 40, no. 4, pp. 481–496, 2001.

[2] K. Wang, J. Deng, Y.-n. Zhang, and C.-p. Wang, "Kinetics and mechanisms of coal oxidation mass gain phenomenon by TG-FTIR and in situ IR analysis," *Journal of Thermal Analysis and Calorimetry*, vol. 132, no. 1, pp. 591–598, 2018.

[3] Q. Lin and J. M. Guet, "Characterization of coals and macerais by X-ray diffraction," *Fuel*, vol. 69, no. 7, pp. 821–825, 1990.

[4] S. Wang, S. Liu, Y. Sun, D. Jiang, and X. Zhang, "Investigation of coal components of late permian different ranks bark coal using AFM and Micro-FTIR," *Fuel*, vol. 187, pp. 51–57, 2017.

[5] J. Ibarra, R. Moliner, and A. J. Bonet, "FT-I.R. investigation on char formation during the early stages of coal pyrolysis," *Fuel*, vol. 73, no. 6, pp. 918–924, 1994.

[6] T. Das, "Evolution characteristics of gases during pyrolysis of maceral concentrates of Russian coking coals," *Fuel*, vol. 80, no. 4, pp. 489–500, 2001.

[7] Q. Shi, B. Qin, Q. Bi, and B. Qu, "An experimental study on the effect of igneous intrusions on chemical structure and combustion characteristics of coal in Daxing Mine, China," *Fuel*, vol. 226, pp. 307–315, 2018.

[8] B. Tian, Y. y. Qiao, Y. y. Tian, and Q. Liu, "Investigation on the effect of particle size and heating rate on pyrolysis characteristics of a bituminous coal by TG-FTIR," *Journal of Analytical and Applied Pyrolysis*, vol. 121, pp. 376–386, 2016.

[9] J. Yu, Y. He, J. Hao et al., "A mathematical model to characterize the degree of coalification based on the low-angle region of the X-ray diffractogram," *Journal of X-Ray Science and Technology*, vol. 26, no. 1, pp. 71–81, 2018.

[10] K. Mae, T. Maki, H. Okutsu, and K. Miura, "Examination of relationship between coal structure and pyrolysis yields using oxidized brown coals having different macromolecular networks," *Fuel*, vol. 79, no. 3-4, pp. 417–425, 2000.

[11] S. Wang, Y. Tang, H. H. Schobert, G. D. Mitchell, F. Liao, and Z. Liu, "A thermal behavior study of Chinese coals with high hydrogen content," *International Journal of Coal Geology*, vol. 81, no. 1, pp. 37–44, 2010.

[12] Q. Sun, W. Li, H. Chen, and B. Li, "The variation of structural characteristics of macerals during pyrolysis⋆," *Fuel*, vol. 82, no. 6, pp. 669–676, 2003.

[13] K. Angoni, "Remarks on the structure of carbon materials on the basis of Raman spectra," *Carbon*, vol. 31, no. 4, pp. 537–547, 1993.

[14] V. Mennelia, G. Monaco, I. Colangeli, and E. Bussoletti, "Raman spectra of carbon based materials excited at 1064 nm," *Carbon*, vol. 33, no. 2, pp. 115–121, 1995.

[15] P. B. Hirsch, "Recent results on the structure of dislocations in tetrahedrally coordinated semiconductors," *Le Journal de Physique Colloques*, vol. 40, no. 6, pp. 6–27, 1979.

[16] I. Watanabe, K. Sakanishi, I. Mochida, and A. Akimoto, "Changes in coal aggregate structure by heat treatment and their coal rank dependency," *Energy & Fuels*, vol. 16, no. 1, pp. 18–22, 2002.

[17] O. O. Sonibare, T. Haeger, and S. F. Foley, "Structural characterization of Nigerian coals by X-ray diffraction, Raman and FTIR spectroscopy," *Energy*, vol. 35, no. 12, pp. 5347–5353, 2010.

[18] W. Zhang, S. Chen, F. Han, and D. Wu, "An experimental study on the evolution of aggregate structure in coals of different ranks by in situ X-ray diffractometry," *Analytical Methods*, vol. 7, no. 20, pp. 8720–8726, 2015.

[19] M. Li, F. Zeng, H. Chang, B. Xu, and W. Wang, "Aggregate structure evolution of low-rank coals during pyrolysis by in-situ X-ray diffraction," *International Journal of Coal Geology*, vol. 116-117, pp. 262–269, 2013.

[20] J. Kister, M. Guiliano, C. Largeau, S. Derenne, and E. Casadevall, "Characterization of chemical structure, degree of maturation and oil potential of Torbanites (type I kerogens) by quantitative FT-I.R. spectroscopy," *Fuel*, vol. 69, no. 11, pp. 1356–1361, 1990.

[21] A. A. Christy, A. L. Hopland, T. Barth, and O. M. Kvalheim, "Quantitative determination of thermal maturity in sedimentary organic matter by diffuse reflectance infrared spectroscopy of asphaltenes," *Organic Geochemistry*, vol. 14, no. 1, pp. 77–81, 1989.

[22] J. Wang, J. Du, L. Chang, and K. Xie, "Study on the structure and pyrolysis characteristics of Chinese western coals," *Fuel Processing Technology*, vol. 91, no. 4, pp. 430–433, 2010.

[23] D. Wu, W. Y. Zhang, B. Fu, and G. Q. Hu, "Chemical structure and gas products of different rank coals during pyrolysis," *Journal of Thermal Analysis and Calorimetry*, vol. 1, pp. 1–15, 2018.

[24] R. M. Bustin, J.-N. Rouzaud, and J. V. Ross, "Natural graphitization of anthracite: experimental considerations," *Carbon*, vol. 33, no. 5, pp. 679–691, 1995.

[25] D. Wu, G. J. Liu, R. Y. Sun, and X. Fan, "Investigation of structural characteristics of thermally metamorphosed coal by FTIR spectroscopy and X-ray diffraction," *Energy Fuels*, vol. 27, no. 10, pp. 5823–5830, 2013.

[26] V. I. José, M. Edgar, and M. Rafael, "FTIR study of the evolution of coal structure during the coalification process," *Organic Geochemistry*, vol. 24, no. 6-7, pp. 725–735, 1996.

[27] S. Yao, K. Zhang, K. Jiao, and W. Hu, "Evolution of coal structures: FTIR analyses of experimental simulations and naturally matured coals in the Ordos basin, China," *Energy Exploration & Exploitation*, vol. 29, no. 1, pp. 1–19, 2011.

[28] A. Bishop and G. D. Abbott, "Vitrinite reflectance and molecular geochemistry of Jurassic sediments: the influence of heating by Tertiary dykes (northwest Scotland)," *Organic Geochemistry*, vol. 22, no. 1, pp. 165–177, 1995.

[29] P. B. Hirsch, "X-ray scattering from coals," *Proceedings of the Royal Society of London. Series A. Mathematical and Physical Sciences*, vol. 226, no. 1165, pp. 143–169, 1954.

[30] A. Arenillas, F. Rubiera, and J. J. Pis, "Simultaneous thermogravimetric-mass spectrometric study on the pyrolysis behaviour of different rank coals," *Journal of Analytical and Applied Pyrolysis*, vol. 50, no. 1, pp. 31–46, 1999.

[31] A. Arenillas, F. Rubiera, C. Pevida, and J. J. Pis, "A comparison of different methods for predicting coal devolatilisation

kinetics," *Journal of Analytical and Applied Pyrolysis*, vol. 58-59, pp. 685–701, 2001.

[32] A. Arenillas, F. Rubiera, J. J. Pis et al., "Thermal behaviour during the pyrolysis of low rank perhydrous coals," *Journal of Analytical and Applied Pyrolysis*, vol. 68-69, pp. 371–385, 2003.

[33] L. Shi, Q. Liu, X. Guo, W. Wu, and Z. Liu, "Pyrolysis behavior and bonding information of coal - a TGA study," *Fuel Processing Technology*, vol. 108, pp. 125–132, 2013.

[34] D. W. Van Krevelen, "Graphical-statistical method for the study of structure and reaction process of coal," *Fuel*, vol. 29, pp. 269–15, 1950.

[35] P. C. Painter, R. W. Snyder, M. Starsinic, M. M. Coleman, D. W. Kuehn, and A. Davis, "Concerning the application of FT-IR to the study of coal: a critical assessment of band assignments and the application of spectral analysis programs," *Applied Spectroscopy*, vol. 35, no. 5, pp. 475–485, 1981.

[36] L. Lu, V. Sahajwalla, C. Kong, and D. Harris, "Quantitative X-ray diffraction analysis and its application to various coals," *Carbon*, vol. 39, no. 12, pp. 1821–1833, 2001.